Caging ruthenium complexes with non-toxic ligands for photoactivated chemotherapy

Cuello Garibo, J.A.

4

Ruthenium-based PACT compounds based on an N,S protecting ligand: a delicate balance between photoactivation and thermal stability

We have shown that sterically hindering bipyridyl molecules such as dmbpy cannot be used as protecting ligands in ruthenium PACT complexes on account of their cytotoxicity. Thus, new non-toxic ligands that provide efficient and selective photosubstitution are investigated. In this chapter, we report on the synthesis, stereochemical characterization, and cytotoxicity of the series of complexes $[Ru(N,N)_2(mtpa)](PF_6)_2$ *where N,N is a bipyridyl ligand and mtpa is 3-(methylthio)propylamine, a non-toxic bidentate N,S ligand. The number of sterically hindering methyl groups increases from zero in* $[Ru(bpy)_2(mtpa)](PF_6)_2$ *(**[1]**$(PF_6)_2$, bpy = 2,2'-bipyridine) to two in* $[Ru(bpy)(dmbpy)(mtpa)](PF_6)_2$ *(**[2]**$(PF_6)_2$, dmbpy = 6,6'-dimethyl-2,2'-bipyridine), and up to four in* $[Ru(dmbpy)_2(mtpa)](PF_6)_2$ *(**[3]**$(PF_6)_2$). The identification of the isomer(s) effectively obtained in solution, including the configuration of the prochiral sulfur, required a combination of crystallography, NOESY spectroscopy, and DFT calculations. The number of methyl groups has a crucial effect on the photochemistry and cytotoxicity of these complexes: while the non-strained complex* $[\mathbf{1}]^{2+}$ *is not capable of fully releasing mtpa and thus is not photocytotoxic against lung cancer cells (A549), the more strained complex* $[\mathbf{2}]^{2+}$ *shows efficient mtpa photosubstitution upon blue light irradiation, leading to photocytotoxicity. However, if the complex is too strained (**[3]**$(PF_6)_2$), it also activates thermally in the dark, losing the photoactivation.*

This chapter has been accepted for publication as a full paper: J. A. Cuello-Garibo, C. James, M. A. Siegler, S. Bonnet, *Chem*^{2}, **2017**, *in press.*

4.1 Introduction

In the last decade, Photoactivated Chemotherapy (PACT) using ruthenium-based complexes has caught attention because it has the potential to control the cytotoxicity of anticancer drugs in space and time. Whereas in Photodynamic Therapy (PDT) cytotoxicity is obtained by the photochemical generation of reactive oxygen species (ROS) such as singlet oxygen,[1-3] in metal-based PACT a new cytotoxic drug is formed *in situ* via photosubstitution of at least one of the ligands of the original prodrug.[4-5] In many reported examples, ruthenium PACT agents are based on complexes of the $[Ru(bpy)_2(dmbpy)]^{2+}$ family, where bpy is 2,2'-bipyridine and dmbpy is the sterically hindering ligand 6,6'-dimethyl-2,2'-bipyridine that increases the distortion of the coordination octahedron.[6-7] In such strained complexes, the triplet metal-centered excited state (^{3}MC) of the complex is lowered and can thus be thermally populated from the photochemically generated triplet metal-to-ligand charge-transfer state (^{3}MLCT), leading to photosubstitution of dmbpy by two solvent molecules. The increased cytotoxicity of the compound after light irradiation was generally attributed to the formation of the bis-aqua complex *cis*-$[Ru(bpy)_2(OH_2)_2]^{2+}$, which was initially proposed to be the cytotoxic species. However, we demonstrated in Chapter 3 that the second photoproduct obtained upon irradiation of $[Ru(bpy)_2(dmbpy)]^{2+}$ in water, *i.e.* the free dmbpy ligand, is the actual cytotoxic species.[8] These findings resulted in the formulation of two questions: first, can we design a light-activated ruthenium complex in which the ruthenium bis-aqua photoproduct is the cytotoxic species? And secondly, if sterically hindering bipyridyl chelates such as dmbpy cannot be used on account of its cytotoxicity, which kind of non-toxic ligands are available, and how can we fine-tune the metal complex to obtain efficient and selective photosubstitution?

In Chapter 2 we have described the use of L-proline as a possible replacement for dmbpy in a series of ruthenium polypyridyl complexes with different steric hindrance.[9] We concluded that, although L-proline was not photosubstituted in water in any case, it could be photosubstituted in more apolar solvents such as CH_3CN if the strain was high enough. This result suggested that photoactivation of such compounds may happen within cancer cells in an apolar environment such as the cell membrane. However, later (*unreported*) high-throughput screening of these complexes against A549 lung cancer cells did not show any cytotoxicity, neither in the dark nor upon light irradiation. Thus, we decided to move from the anionic N,O chelating ligand L-proline to neutral N,S chelating ligands. Our group actively investigates the use of thioether ligands for the caging of aquated ruthenium complexes.[10] Thioethers are excellent ligands for

ruthenium(II) due to their softness, which often leads to thermally stable complexes. In addition, many ruthenium complexes coordinated to thioethers show selective photosubstitution of the thioether ligand by solvent molecule(s) upon visible light irradiation.[11-12] For example, we have shown in Chapter 3 that complexes $[Ru(bpy)_2(mtmp)]Cl_2$ and $[Ru(Ph_2phen)_2(mtmp)]Cl_2$ (where Ph_2phen = 4,7-diphenyl-1,10-phenanthroline and mtmp = 2-(methylthio)methylpyridine) can efficiently photosubstitute the non-toxic N,S chelating ligand mtmp by two solvent molecules in water. When A549 cells were treated with the two complexes and irradiated with light, only the more lipophilic complex $[Ru(Ph_2phen)_2(mtmp)]Cl_2$ showed a strong cytotoxicity characterized by an EC_{50} value in the submicromolar range, as $[Ru(bpy)_2(mtmp)]Cl_2$ could not enter the cells. $[Ru(Ph_2phen)_2(mtmp)]Cl_2$ was, unfortunately, also very toxic in the dark (EC_{50} ~ 2.7 μM), probably due to its high lipophilicity. Thus, a different strategy to fine-tune the lipophilicity of these compounds is now introduced, which consists in varying the number of methyl substituents in the spectator bpy ligands. In this work, we report on the synthesis and stereochemical characterization of the series of complexes $[Ru(bpy)_2(mtpa)](PF_6)_2$ ([**1**]$(PF_6)_2$), $[Ru(bpy)(dmbpy)(mtpa)](PF_6)_2$ ([**2a**]$(PF_6)_2$ and [**2b**]$(PF_6)_2$), and $[Ru(dmbpy)_2(mtpa)](PF_6)_2$ ([**3**]$(PF_6)_2$), where mtpa is 3-(methylthio)propylamine, a dissymmetric bidentate ligand derived from methionine by decarboxylation (Figure 4.1). The number of sterically hindering methyl groups increases from zero in [**1**]$(PF_6)_2$ to two in [**2a**]$(PF_6)_2$ and [**2b**]$(PF_6)_2$, and up to four in [**3**]$(PF_6)_2$. Next to increasing steric hindrance, more methyl groups also increase the lipophilicity of the complex, and hence its ability to cross membranes in the cells. The effect of the number of methyl groups on the photochemistry and cytotoxicity of these complexes is discussed.

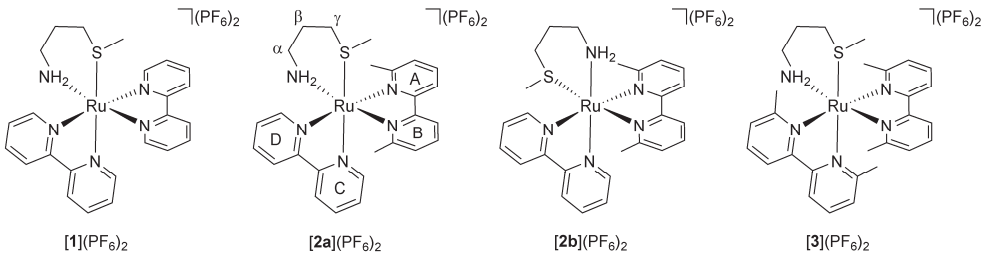

*Figure 4.1. Structures of the complexes [**1**](PF$_6$)$_2$, [**2a**](PF$_6$)$_2$, [**2b**](PF$_6$)$_2$, and [**3**](PF$_6$)$_2$. The configuration of the sulfur center is not specified. For clarity only the Λ isomers are shown, but all samples were obtained as racemic Δ/Λ mixtures.*

4.2 Results

4.2.1 Synthesis

A series of three ruthenium complexes with zero, two, or four methyl groups on the bpy ligands was synthesized (Figure 4.1). Complexes [**1**]$(PF_6)_2$ and [**3**]$(PF_6)_2$ were obtained in a similar manner by reacting their precursors $[Ru(bpy)_2Cl_2]$ and $[Ru(dmbpy)_2Cl_2]$ with the mtpa ligand, to afford racemic mixtures in both cases. Besides the chirality of the octahedron (Δ or Λ), two other sources of isomerism are present (Scheme 4.1): the configuration (*S* or *R*) of the sulfur atom, and the chair inversion of the six-membered ring resulting from the coordination of the N,S chelating ligand to the ruthenium center, which transforms an axial thioether methyl group (*ax*) into an equatorial one (*eq*) and *vice versa*. This isomerism leads to a total of four possible isomers, *i.e.* Λ-(*R*)-*eq*-[**Ru**]$^{2+}$, Λ-(*R*)-*ax*-[**Ru**]$^{2+}$, Λ-(*S*)-*eq*-[**Ru**]$^{2+}$, and Λ-(*S*)-*ax*-[**Ru**]$^{2+}$ (where [**Ru**]$^{2+}$ is either [**1**]$^{2+}$, [**2a**]$^{2+}$, [**2b**]$^{2+}$, or [**3**]$^{2+}$), together with their enantiomers Δ-(*S*)-*eq*-[**Ru**]$^{2+}$, Δ-(*S*)-*ax*-[**Ru**]$^{2+}$, Δ-(*R*)-*eq*-[**Ru**]$^{2+}$, and Δ-(*R*)-*ax*-[**Ru**]$^{2+}$, respectively. As shown in Scheme 4.1, inversion of the chair does not change the configuration (*S* or *R*) of the chiral sulfur center but the conformation of the chair, thus changing the position of the methyl substituent from equatorial (*eq*) to axial (*ax*) or *vice versa*. According to the signals of ^{1}H NMR, complexes [**1**]$(PF_6)_2$ and [**3**]$(PF_6)_2$ were obtained as a mixture of two diastereoisomers, with ratios of 1:0.05 and 1:0.12, respectively. The temperature-dependent ^{1}H NMR spectrum of [**1**]$(PF_6)_2$ in CD_3OD did not show any significant difference at 193 K, 293 K, and 333 K, refuting the hypothesis that inversion of the sulfur from *R* to *S* or *vice versa* may be fast at room temperature, and confirming that two stable diastereoisomers have been obtained for [**1**]$^{2+}$ and by extension for [**3**]$^{2+}$. On the other hand, a previously reported synthetic route was used to synthesize [**2**]$(PF_6)_2$,[9] which consisted first in preparing *cis*-$[Ru(bpy)(dmbpy)(CH_3CN)_2](PF_6)_2$ ([**4**]$(PF_6)_2$) by visible light irradiation of the precursor $[Ru(bpy)(dmbpy)_2](PF_6)_2$ ([**5**]$(PF_6)_2$) in CH_3CN, and then reacting [**4**]$(PF_6)_2$ with mtpa in water. The ^{1}H NMR spectrum of the crude product of [**2**]$(PF_6)_2$ showed two doublets at 9.55 and 9.17 ppm, characteristic for the hydrogen in position 6 or 6' on the bpy, in a ratio of 1:0.55. Mass spectrometry showed peaks at m/z = 273.2, 287.4, and 692.0, which correspond to $[Ru(bpy)(dmbpy)(mtpa)]^{2+}$ (calcd m/z = 273.6), $[Ru(dmbpy)_2(mtpa)]^{2+}$ (calcd m/z = 287.6), and $\{[Ru(bpy)(dmbpy)(mtpa)](PF_6)\}^+$ (calcd m/z = 692.1), respectively, indicating the occurrence of ligand scrambling. Since the two doublets in the 9−10 ppm range cannot belong to $[Ru(dmbpy)_2(mtpa)]^{2+}$, the two main species present in the mixture share the same mass peaks, *i.e.* they are two of

the expected isomers of $[\mathbf{2}]^{2+}$. Resolution of both isomers by alumina column chromatography using a mixture of CH_2Cl_2/CH_3OH (99:1) as eluent did produce a main fraction containing both isomers in a ratio 1:0.07 according to ^{1}H NMR.

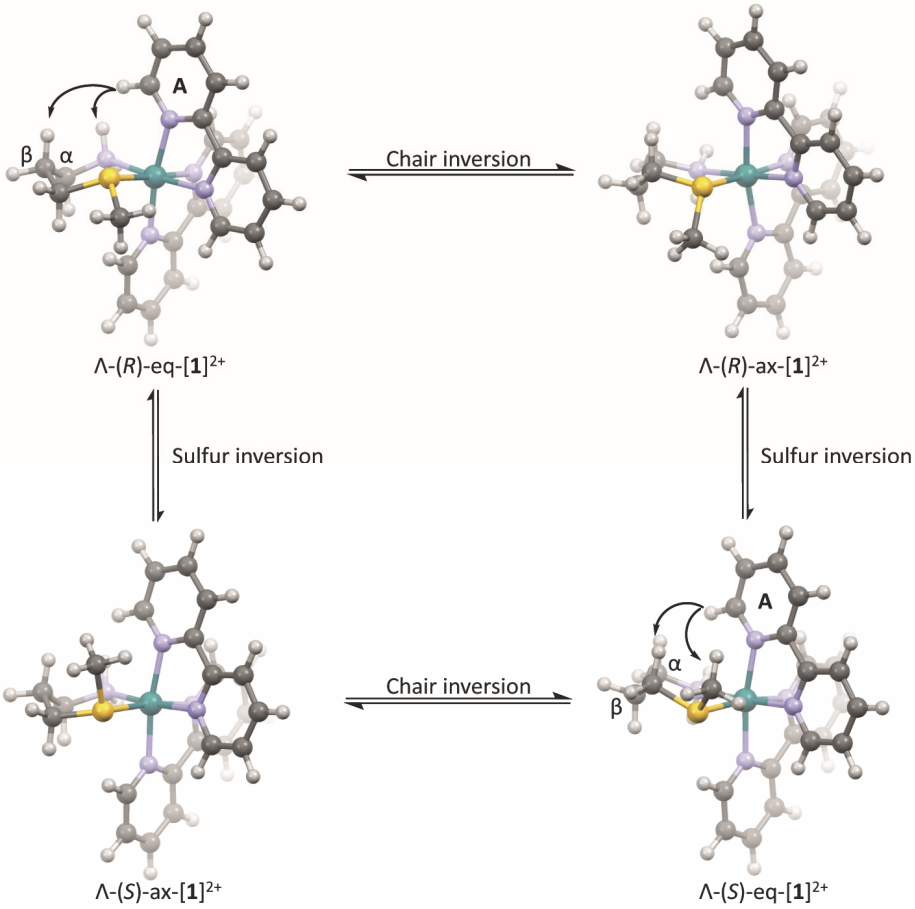

Scheme 4.1. Isomers of $[\mathbf{1}]^{2+}$ as a result of the inversion of either the chirality of the sulfur atom (R or S) or the conformation of the chair. Isomers Λ-(R)-eq-$[\mathbf{1}]^{2+}$ and Λ-(S)-eq-$[\mathbf{1}]^{2+}$ show distances between N_{eq} and A6 of 3.398 and 2.585 Å, respectively, and distances between the α_{ax} and A6 of 4.638 and 1.983 Å, respectively.

The tris-heteroleptic complex $[\mathbf{2}](PF_6)_2$ bears three different bidentate ligands, thus the two different orientations of mtpa lead to two different regioisomers: either (OC-6-43)-[Ru(bpy)(dmbpy)(mtpa)]$^{2+}$, in which the thioether sulfur donor is *trans* to the bpy, or (OC-6-34)-[Ru(bpy)(dmbpy)(mtpa)]$^{2+}$, in which the thioether ligand is *trans* to the dmbpy ligand. For simplicity, these two regiosiomers are called $[\mathbf{2a}](PF_6)_2$ and $[\mathbf{2b}](PF_6)_2$, respectively (Figure 4.1). Like for $[\mathbf{1}](PF_6)_2$ and $[\mathbf{3}](PF_6)_2$, each of the regioisomers of $[\mathbf{2}](PF_6)_2$ has four possible isomers, which leads to a total of eight

possible Λ diastereoisomers and their corresponding eight Δ enantiomers. NOESY analysis in D_2O showed an off-diagonal correlation between a proton of the amine and the methyl substituent on the dmbpy for the major isomer, which means that in this isomer the amine must be *trans* to dmbpy. Thus, the major isomer in this fraction was $[\mathbf{2a}]^{2+}$, while the minor isomer remains unassigned. However, after storage for two weeks as a powder in the freezer (−20 °C), this purified sample had isomerized back into a 1:0.4 mixture of isomers, which showed that isomerization was occurring even under such conditions, and thus that the two isomers cannot be kept in separate flasks. Below, $[\mathbf{2}](PF_6)_2$ is used as a mixture of these two regioisomers.

4.2.2 Characterization by DFT and NOESY studies

In order to understand the stereoselectivity of sulfur coordination in solution, Density Functional Theory (DFT) calculations of complexes $[\mathbf{1}]^{2+}$, $[\mathbf{2a}]^{2+}$, $[\mathbf{2b}]^{2+}$, and $[\mathbf{3}]^{2+}$ were performed in water using the COSMO model for simulating solvent effects (see Experimental Section). In each case only the Λ enantiomer having the six-membered ring in a chair conformation was modelled. The sulfur atom was either in *R* or *S* configuration, with the methyl group either in equatorial or in axial position by inversion of the chair, following Scheme 4.1 and resulting in a total of four possible isomers per complex. The optimized structures and their energies in water are given in Scheme 4.1, Figure AV.11, Figure AV.12, and Table 4.1, respectively. Complex Λ-(*S*)-*eq*-$[\mathbf{1}]^{2+}$ is the lowest in energy, followed by Λ-(*S*)-*ax*-$[\mathbf{1}]^{2+}$ at +5.4 kJ·mol^{-1}, obtained by inversion of the chair. NOESY analysis of $[\mathbf{1}](PF_6)_2$ in D_2O showed an off-diagonal correlation between the A6 proton on bpy and the N_{eq} proton of mtpa, and a correlation between A6 and the α_{ax} proton (Figure AV.1). In the calculated structure of Λ-(*R*)-*eq*-$[\mathbf{1}]^{2+}$ the distances between those atoms are 3.398 and 4.638 Å, respectively, whereas in Λ-(*S*)-*eq*-$[\mathbf{1}]^{2+}$ the distances are much shorter, *i.e.* 2.585 and 1.983 Å, respectively (Figure 4.2). Thus, altogether the DFT and NMR studies suggest that $[\mathbf{1}]^{2+}$ in solution is a racemic mixture containing Λ-(*S*)-*eq*-$[\mathbf{1}]^{2+}$ and Δ-(*R*)-*eq*-$[\mathbf{1}]^{2+}$, which are also the most thermodynamically stable pair of enantiomers.

Table 4.1. Absolute and relative energies in water (COSMO) of the isomers of $[\mathbf{1}]^{2+}$, $[\mathbf{2a}]^{2+}$, $[\mathbf{2b}]^{2+}$, *and* $[\mathbf{3}]^{2+}$ *optimized by DFT/PBE0/TZP.*

Isomer	Absolute energy in water (Hartree)	Relative energy ΔE in water ($kJ \cdot mol^{-1}$)
Λ-(*R*)-*eq*-[1]$^{2+}$	−16.23684667	6.4
Λ-(*R*)-*ax*-[1]$^{2+}$	−16.23341885	15.4
Λ-(*S*)-*eq*-[1]$^{2+}$	−16.23930307	0.0
Λ-(*S*)-*ax*-[1]$^{2+}$	−16.23723835	5.4
Λ-(*R*)-*eq*-[2a]$^{2+}$	−17.67935607	0.0
Λ-(*R*)-*ax*-[2a]$^{2+}$	−17.67277958	17.3
Λ-(*S*)-*eq*-[2a]$^{2+}$	−17.67921051	0.4
Λ-(*S*)-*ax*-[2a]$^{2+}$	−17.67779925	4.1
Λ-(*R*)-*eq*-[2b]$^{2+}$	−17.67166128	20.2
Λ-(*R*)-*ax*-[2b]$^{2+}$	−17.66922670	26.6
Λ-(*S*)-*eq*-[2b]$^{2+}$	−17.67649787	7.5
Λ-(*S*)-*ax*-[2b]$^{2+}$	−17.67485691	11.8
Λ-(*R*)-*eq*-[3]$^{2+}$	−19.12274771	8.4
Λ-(*R*)-*ax*-[3]$^{2+}$	−19.11917987	17.7
Λ-(*S*)-*eq*-[3]$^{2+}$	−19.11171121	37.3
Λ-(*S*)-*ax*-[3]$^{2+}$	−19.12592873	0.0

For the tris-heteroleptic complex [**2**]$^{2+}$, isomer Λ-(*R*)-*eq*-[**2a**]$^{2+}$ appeared to be the most stable in water according to DFT, followed by the other isomers of [**2a**]$^{2+}$. The isomers of [**2b**]$^{2+}$ were found at higher energies, ranging from +7.5 to +26.6 $kJ \cdot mol^{-1}$. Furthermore, NOESY analysis in CD_3OD shows an off-diagonal correlation between the D6 proton on the bpy of the major isomer with both MeS- and the γ proton of mtpa (Figure AV.2). In the calculated structure of Λ-(*R*)-*eq*-[**2a**]$^{2+}$ the distances between those atoms are short (2.083 and 2.147 Å, respectively, see Figure 4.2), whereas in Λ-(*S*)-*eq*-[**2a**]$^{2+}$ the distances are larger, being 4.198 and 3.918 Å, respectively. Thus, NMR data agree with DFT that the major and most stable isomer is Λ-(*R*)-*eq*-[**2a**]$^{2+}$. Meanwhile, DFT calculations suggest that the minor isomer would correspond to Λ-(*S*)-*eq*-[**2a**]$^{2+}$ if the formation of [**2**]$^{2+}$ would be under thermodynamic control. Unfortunately, it was impossible to isolate the minor isomer and to confirm this hypothesis. Finally, for the most strained complex of the series, isomer Λ-(*S*)-*ax*-[**3**]$^{2+}$ was the most stable according to DFT, followed by Λ-(*R*)-*eq*-[**3**]$^{2+}$, Λ-(*R*)-*ax*-[**3**]$^{2+}$, and Λ-(*S*)-*eq*-[**3**]$^{2+}$ at +8.4, +17.7, and +37.3 $kJ \cdot mol^{-1}$, respectively. NOESY analysis in

CD_3OD showed an off-diagonal correlation between the methyl substituent DMe and the proton γ_{ax}, and another correlation between the methyl substituent AMe and the methyl of the thioether group, with a relative intensity of the signals of 65% and 35%, respectively (Figure AV.3). According to the calculated structures, the distances between those hydrogens are 3.439 and 3.102 Å in Λ-(*S*)-*eq*-[**3**]$^{2+}$, 2.133 and 6.246 Å in Λ-(*R*)-*eq*-[**3**]$^{2+}$, and 2.127 and 2.995 Å in Λ-(*S*)-*ax*-[**3**]$^{2+}$, respectively (Figure 4.2). Thus, isomer Λ-(*S*)-*ax*-[**3**]$^{2+}$, observed in the crystal structure, fits best the obtained NOESY data in solution. Overall, irrespective of the steric hindrance the major isomer in solution in this series of complexes is the most stable one according to DFT calculations.

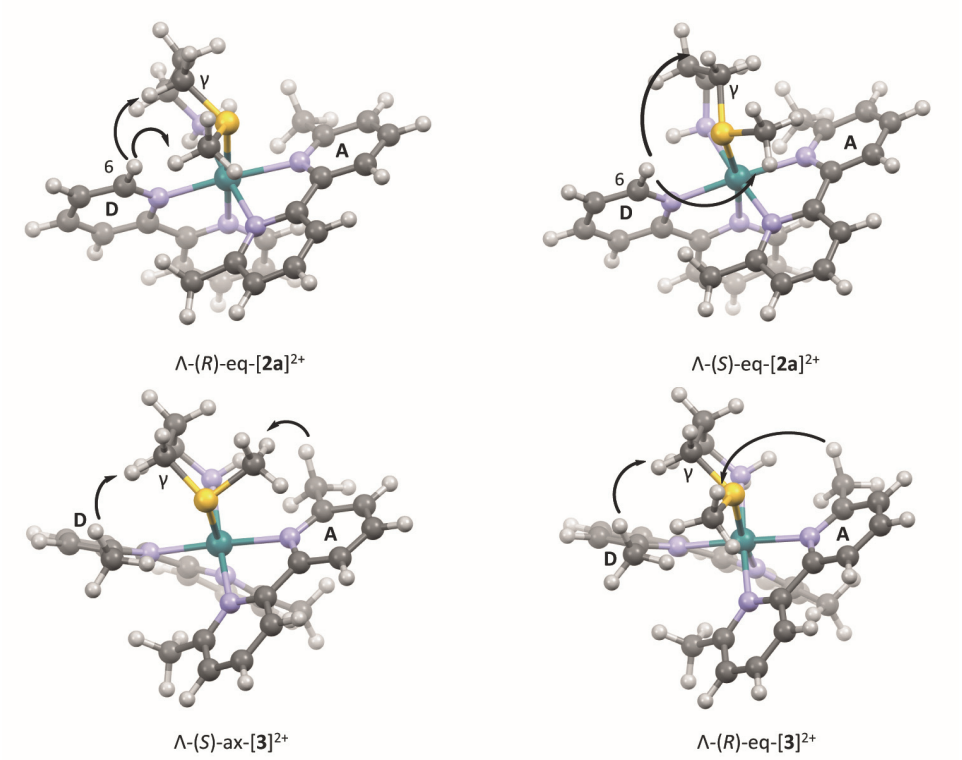

*Figure 4.2. Structures of selected isomers of [**2**]$^{2+}$ and [**3**]$^{2+}$ optimized by DFT in water (COSMO). Isomers Λ-(R)-eq-[**2a**]$^{2+}$ and Λ-(S)-eq-[**2a**]$^{2+}$ show distances between γ_{ax} and D6 of 2.147 and 3.918 Å, respectively, and distances between the methyl thioether group and D6 of 2.083 and 4.198 Å, respectively. Isomers Λ-(S)-ax-[**3**]$^{2+}$ and Λ-(R)-eq-[**3**]$^{2+}$ show distances between γ_{ax} and DMe of 2.127 and 2.133 Å, respectively, and distances between the methyl thioether group and AMe of 2.995 and 6.246 Å, respectively*

To quantify steric hindrance in this series of complexes, the structural distortion parameter,[13] *i.e.* the bond angle variance (σ^2), was calculated from the DFT models for

all the isomers with the methyl group in equatorial position as well as for Λ-(*S*)-*ax*-[**3**]$^{2+}$ (Table AV.1). In a simple assumption, more strained molecules should have a more distorted coordination octahedron, thus a higher σ^2 value. However, the change in the configuration of the sulfur atom appears to have a great impact on σ^2. All the isomers with *R* configuration were found to have a higher σ^2 value than their corresponding *S* isomer (*e.g.* σ^2 is 62.4 and 45.0 for Λ-(*R*)-*eq*-[**1**]$^{2+}$ and Λ-(*S*)-*eq*-[**1**]$^{2+}$, respectively). The σ^2 value for the tris-heteroleptic *R* complex Λ-(*R*)-*eq*-[**2a**]$^{+}$ is even higher than that of the, in principle, more strained *S* complex Λ-(*S*)-*eq*-[**3**]$^{+}$ (81.8 *vs* 76.3). Thus, the orientation of specific bulky moieties such as MeS- has a greater effect on the distortion of the octahedron than the overall number of methyl groups. Furthermore, a direct relation between σ^2 and their DFT-calculated energies in water was found only for the non-strained complex [**1**]$^{2+}$. Indeed, for this complex the least distorted isomer Λ-(*S*)-[**1**]$^{2+}$ was found to have the lowest energy. For complex [**2**]$^{2+}$ the most distorted isomer (Λ-(*R*)-*eq*-[**2a**]$^{2+}$) has the lowest energy in water, whereas for complex [**3**]$^{2+}$ isomers Λ-(*S*)-*ax*-[**3**]$^{2+}$ and Λ-(*S*)-*eq*-[**3**]$^{2+}$, having similar σ^2 values (76.0 and 76.3, respectively), showed the greatest difference in energy (37.3 kJ·mol^{-1}). Since a correlation between octahedral distortion and stability could not be drawn, the interligand repulsion between the methyl substituents and mtpa was also considered. We found that all the isomers that have the H_{ax} in positions 3 and 5 of the six-membered chair facing directly the methyl substituent in the 6 position of the dmbpy ligand, are always higher in energy. As shown in Figure 4.3, for complex Λ-(*S*)-*eq*-[**3**]$^{2+}$, which is the least stable of the isomers of [**3**]$^{2+}$ in water, the distances between H_{ax} in positions 3 and 5 and their spatially closest methyl substituents are only 2.097 and 1.860 Å, respectively. Overall, two factors influence the stability of these complexes and the stereoselectivity of the coordination of mtpa: the octahedral distortion and the interligand repulsion. In the case of the non-strained complex [**1**]$^{2+}$ only the octahedral distortion plays a role, whereas when hindering methyl substituents are introduced in the complex, interligand repulsion becomes the driving force for the stereoselectivity of the reaction.

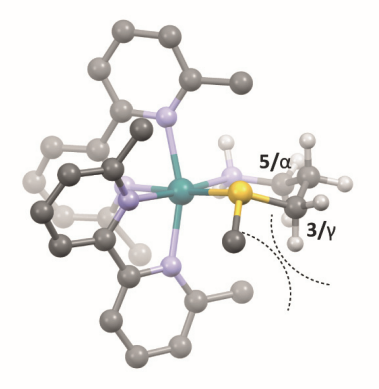

*Figure 4.3. Schematic drawing of isomer Λ-(S)-eq-[**3**]$^{2+}$ showing the steric effect between the methyl substituent on dmbpy facing directly the H_{ax} in positions 3 and 5 of the six-membered ring in a chair conformation.*

4.2.3 X-Ray crystallography

Single crystals suitable for X-Ray structure determination were obtained for complexes [**1**]$(PF_6)_2$, [**2a**]$(PF_6)_2$, and [**3**]$(PF_6)_2$ by slow vapor diffusion of the solvent of a methanol solution of the complex into toluene, ethyl acetate, and di-*tert*-butyl ether, respectively. For complex [**1**]$(PF_6)_2$ the structure contains two enantiomers Λ-(*S*) and Δ-(*R*) of [Ru(bpy)$_2$(mtpa-κN,κS)]$(PF_6)_2 \cdot CH_3OH$. The molecular structure, shown in Figure 4.4a, shows a methyl group in equatorial position, obtaining Λ-*(S)-eq*-[**1**]$(PF_6)_2$, the same isomer suggested by NMR and DFT data in solution. Although [**2**]$(PF_6)_2$ was crystallized using a mixture of two regioisomers, the crystal structure contains a racemate of a single isomer of [**2a**]$(PF_6)_2$ in the orthorhombic space group Pbca, containing both configurations Λ-*(R)* and Δ-*(S)*. The molecular structure shown in Figure 4.4b shows a longer Ru-S bond (2.3668(7) Å) compared to that in Λ-*(S)-eq*-[**1**]$^{2+}$ (2.3314(7) Å, Table 4.2) and the mtpa amine is located *trans* to the dmbpy ligand, confirming the NMR assignment in solution. The methyl group is found to be in equatorial position, thus the crystallized isomer is Λ-*(R)-eq*-[**2a**]$(PF_6)_2$, the same isomer suggested by NMR and DFT data in solution. Finally, [**3**]$(PF_6)_2$ crystallized in a triclinic P-1 space group having an inversion point, and contains the racemate Λ-*(S)* and Δ-*(R)* [**3**]$(PF_6)_2$. The structure shown in Figure 4.4c shows the longest Ru-S bond (2.3845(8) Å) of the series. Thus, more methyl groups in the complex lead to longer Ru-S bonds but do not affect Ru-N bonds distances. The methyl group of the thioether is in axial position, resulting in the isomer Λ-*(S)-ax*-[**3**]$(PF_6)_2$, the same isomer suggested by NMR and DFT data in solution. Interestingly, whereas for complex [**1**]$(PF_6)_2$ and [**3**]$(PF_6)_2$ the obtained structures have the configuration Λ-*(S)* and Δ-*(R)*,

in [**2a**]$(PF_6)_2$ they are Λ-*(R)* and Δ-*(S)*. In every case, the six-membered ring resulting from the coordination of mtpa to the ruthenium center is in a chair conformation, as modelled in the DFT calculations. Furthermore, comparing the structures of Λ-*(S)*-[**1**]$(PF_6)_2$ and Λ-*(R)*-[**2**]$(PF_6)_2$ a flip in the chair conformation accompanied the change in the configuration of the sulfur atom from (*S*) to (*R*), probably in order to keep the methyl group in the equatorial position.

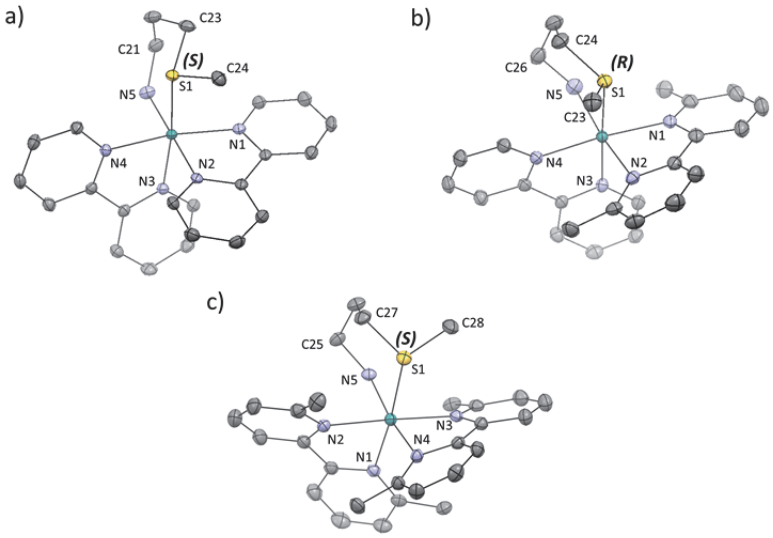

*Figure 4.4. Displacement ellipsoid plot (50% probability level) of the cationic complex in the crystal structure of the Λ enantiomer of a) Λ-(S)-eq-[**1**]$(PF_6)_2$, b) Λ-(R)-eq-[**2a**]$(PF_6)_2$, and c) Λ-(S)-ax-[**3**]$(PF_6)_2$. Hexafluoridophosphate counteranions, hydrogen atoms, lattice CH_3OH (in the case of [**1**]$(PF_6)_2$), and disorder have been omitted for clarity.*

*Table 4.2. Selected bond lengths (Å) and angles (°) for Λ-(S)-eq-[**1**]$(PF_6)_2$, Λ-(R)-eq-[**2a**]$(PF_6)_2$, and Λ-(S)-ax-[**3**]$(PF_6)_2$.*

	Λ-(*S*)-*eq*-[1]$(PF_6)_2$	**Λ-(*R*)-*eq*-[2a]$(PF_6)_2$**	**Λ-(*S*)-*ax*-[3]$(PF_6)_2$**
Ru1-S1	2.3314(7)	2.3668(7)	2.3845(8)
Ru1-N1	2.079(2)	2.117(2)	2.102(2)
Ru1-N2	2.066(2)	2.112(2)	2.113(2)
Ru1-N3	2.079(2)	2.064(2)	2.087(2)
Ru1-N4	2.083(2)	2.081(2)	2.087(2)
Ru1-N5	2.149(2)	2.167(2)	2.164(2)
S1-C23-C21-N5	−12.8(2)	-	-
S1-C24-C26-N5	-	−8.1(2)	-
S1-C25-C27-N5	-	-	−4.7(2)

4.2.4 Photochemistry and thermal stability

The photoreactivity and thermal stability of all the complexes was studied in water and monitored with a variety of techniques including ^{1}H NMR, UV-vis spectroscopy, and mass spectrometry. Complex [**1**](PF$_6$)$_2$, when irradiated with blue light (445 nm), showed a bathochromic shift in the ^{1}MLCT band with a change in the maximum absorption from 450 nm to 486 nm, and clear isosbestic points at 325 nm, 390 nm, and 460 nm, indicating a one-step process (Figure 4.5a). After 6 min at ~$3\cdot10^{-8}$ mol·s^{-1} photon flux the photoreaction had reached the steady state. Mass spectrometry performed at that point showed major peaks at m/z = 260.0, 269.0, and 536.2, corresponding to [Ru(bpy)$_2$(mtpa)]$^{2+}$ (calcd m/z = 259.6), [Ru(bpy)$_2$(mtpa)(OH$_2$)]$^{2+}$ (calcd m/z = 268.6), and [Ru(bpy)$_2$(mtpa)(OH)]$^{+}$ (calcd m/z = 536.1), respectively, but no peaks corresponding to the bis photosubstituted species [Ru(bpy)$_2$(OH$_2$)$_2$]$^{2+}$ (calcd m/z = 225.03, Figure AV.6). Thus, only one coordination position was substituted by a water molecule and it appeared impossible to reach full conversion, since peaks belonging to the starting compound [**1**](PF$_6$)$_2$ were still present at the steady state. As shown in Figure 4.6b, when the same photoreaction was monitored with NMR in D$_2$O, doublets at 9.79 and 9.24 ppm, characteristic of hydrogens in positions 6 and 6' of bpy in [**1**](PF$_6$)$_2$, decreased in intensity after 40 min, whereas new doublets at 9.23 and 9.21 ppm arose for the photoproduct, reaching the steady state with a ratio of 3.4:1 between the photoproduct and the starting complex. Furthermore, the singlet peak of the methyl thioether shifted downfield from 1.20 to 1.92 ppm, which is characteristic for a free methyl thioether. Thus, as shown in Scheme 4.2, the sulfur moiety was photosubstituted, but the amine ligand stayed bound, *i.e.* the photoproduct is [Ru(bpy)$_2$(mtpa-κN)(OH$_2$)]$^{2+}$. Furthermore, when the photoproduct was kept in the dark at room temperature, the reverse reaction took place very slowly, with the doublets at 9.23 and 9.21 ppm, characteristic of [**1**](PF$_6$)$_2$, increasing again after 30 days (Figure 4.6b). The reversibility of the ring opening photoreaction was also studied using UV-vis spectroscopy by irradiating [**1**](PF$_6$)$_2$ four times during 5 min, each time followed by ~2 h of equilibration in the dark at 37 °C (to increase the rate of back coordination). As shown in Figure 4.6a, the ring opening is clearly reversible. Photosubstitution of only one monodentate amine or pyridine ligand L in ruthenium [Ru(bpy)$_2$(L)$_2$]$^{2+}$ complexes is classical in literature,[14-15] as well as hemilability followed by either fast rechelation (also called recaptation) or full dissociation of the bidentate ligand.[16-18] However, hemilability followed by such a slow rechelation is rare. Here, it appears to be a consequence of the difference in binding properties between the thioether and amine donor atoms. Thus, complex [**1**]$^{2+}$ shows a light-

controlled Ru-S bond breaking and thermal recovery, *i.e.* it behaves like a photoswitch (Scheme 4.2).

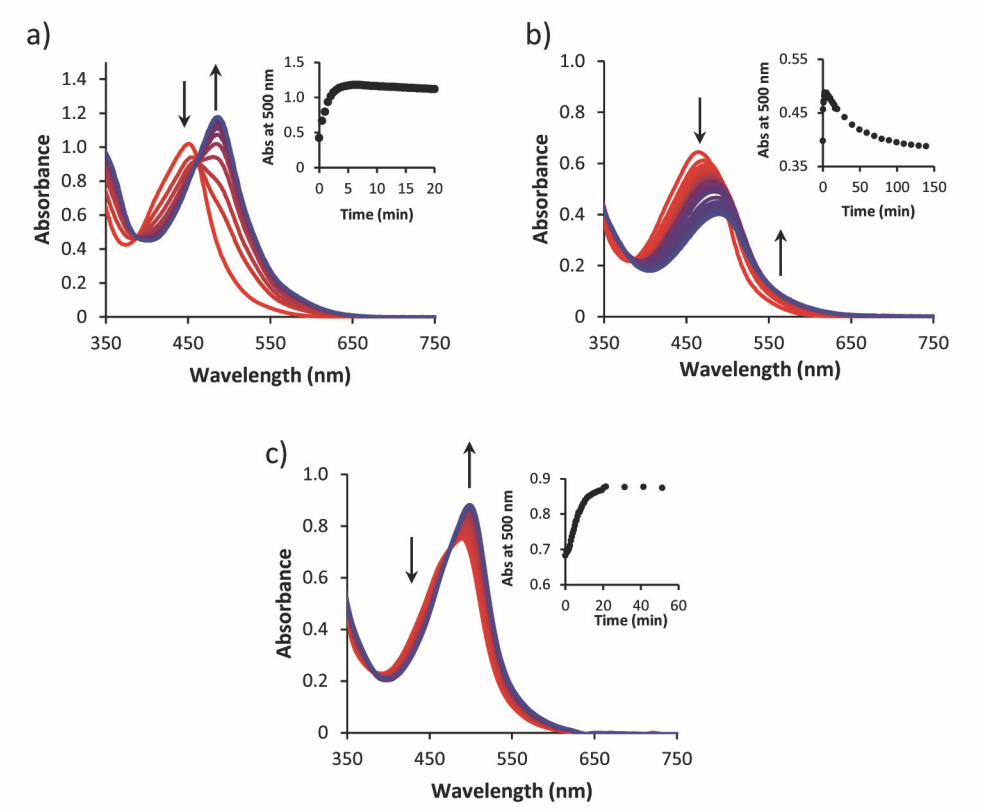

*Figure 4.5. Evolution of the UV-vis spectra of water solutions of (a) [**1**](PF$_6$)$_2$ (0.145 mM), (b) [**2**](PF$_6$)$_2$ (0.101 mM), and (c) [**3**]Cl$_2$ (0.123 mM) upon irradiation with a 445 nm LED (2.9 ± 0.1·10^{-8} mol·s^{-1}) under N$_2$ at 25 °C. Insets: evolution of the absorbance at 500 nm vs. time.*

The photoreactivity of the most strained complex [**3**]$^{2+}$ was studied in water for comparison. First, [**3**](PF$_6$)$_2$ was converted to the chloride salt [**3**]Cl$_2$ to increase water solubility. When a solution of [**3**]Cl$_2$ in water was irradiated with a 445 nm LED a change in the MLCT band of the UV-vis spectra was observed, with a small bathochromic shift of the maximum absorption to 500 nm (Figure 4.5c). The steady state was reached after 20 min irradiation at the same photon flux as above (~3·10^{-8} mol·s^{-1}). A mass spectrum of the irradiated sample showed no peaks that would correspond to the starting complex (Figure AV.8). When a solution of [**3**]Cl$_2$ was kept in the dark and monitored with UV-vis, a qualitatively similar but less pronounced change in the spectra was observed. When [**3**]Cl$_2$ was dissolved in D$_2$O to monitor the photoreaction with ^{1}H NMR, two sets of peaks were present already at t = 0 h, with a doublet at 7.22 ppm (integrating for two H, characteristic of the

hydrogen at position 3 in the dmbpy), and two doublets at 7.30 and 7.35 ppm (integrating for one H each), indicating the presence of two species in a ratio of 1:0.5 (Figure AV.5a). When this mixture was kept in the dark at room temperature for 72 h, almost no change was observed. However, when the solution was irradiated with a Xe lamp mounted with a 450 nm bandpass filter, the doublets at 7.30 and 7.35 ppm disappeared after 3 h, whereas the intensity of the doublet at 7.22 ppm increased (Figure AV.5b). This peak belongs to the solvated complex $[Ru(dmbpy)_2(OH_2)_2]^{2+}$. Thus, [**3**]$(PF_6)_2$ in water is not stable in the dark. The mtpa ligand is substituted by two water molecules, to reach an equilibrium between $[\mathbf{3}]^{2+}$ and $[Ru(dmbpy)_2(OH_2)_2]^{2+}$ (Scheme 4.2). This equilibrium can be displaced by light irradiation, as has been reported for other types of strained ruthenium complexes.[11, 19]

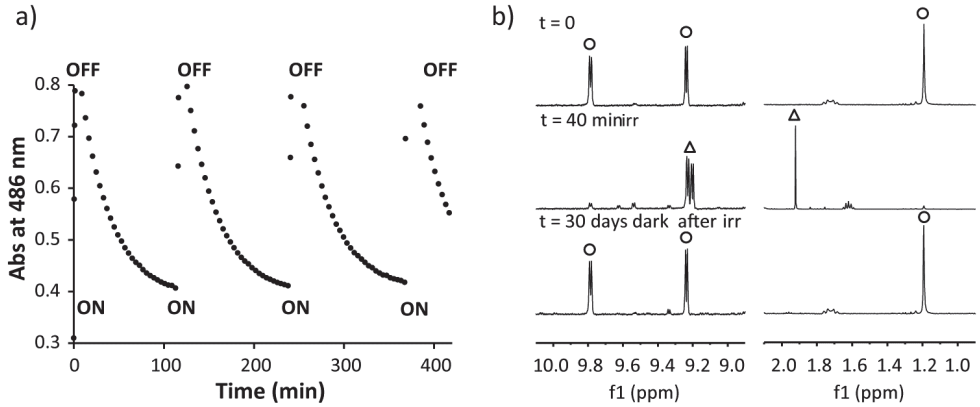

*Figure 4.6. a) Evolution of the absorbance at 486 nm vs. time of a solution of [**1**]$(PF_6)_2$ in water (0.099 mM) upon switching ON and OFF several times a source of blue light (λ_e = 445 nm, $2.9 \cdot 10^{-8}$ mol·s^{-1}) at 310 K under N_2. b) Evolution of the ^{1}H NMR spectra (regions 10 – 9 ppm and 2 – 1 ppm) of a solution of [**1**]$(PF_6)_2$ in D_2O (3.04 mM) irradiated with a Xe lamp for 40 min (ON) and then left in the dark for 30 days (OFF) at room temperature. The doublets at 9.79 and 9.24 ppm (circles) correspond to the H_6 protons on the bpy for complex $[\mathbf{1}]^{2+}$ and the arising doublets at 9.23 and 9.21 ppm (triangle) correspond to the H_6 proton on the bpy for the monodentate-bound mtpa ligand in $[Ru(bpy)_2(mtpa\text{-}\kappa N)(OH_2)]^{2+}$. The singlet at 1.20 ppm (circles) corresponds to the methyl thioether group, and the arising singlet at 1.92 ppm (triangle) corresponds to the decoordinated thioether.*

Finally, the photoreactivity of the moderately strained complex [**2**]$(PF_6)_2$ was investigated by irradiating a solution of [**2**]$(PF_6)_2$ in water with a 445 nm LED. UV-vis spectra showed a bathochromic shift of the absorption maximum from 464 nm to 492 nm, without any clear isosbestic point in the MLCT region (Figure 4.5b). Mass spectra after completion of the photoreaction showed peaks at m/z = 261.9 and 222.5, corresponding to $[Ru(bpy)(dmbpy)(CH_3CN)_2]^{2+}$ (calcd m/z = 262.1) and $[Ru(bpy)(mtpa)(CH_3CN)_2]^{2+}$ (calcd m/z = 222.5, Figure AV.7), respectively, which means that both dmbpy and mtpa ligands are photosubstituted in two parallel

photoreactions. The CH_3CN molecules come from the eluent used for the mass spectrometry as irradiation was performed in water. To confirm that photosubstitution of both mtpa and dmbpy occurred, white light irradiation of a solution of [**2**]$(PF_6)_2$ in D_2O was monitored by ^1H NMR. As shown in Figure AV.4, after 60 min the doublet of the starting complex at 9.57 ppm completely vanished, while three new doublets appeared in the 9.00 – 10.00 ppm range, at 9.72, 9.38, and 9.21 ppm in a 1:1:0.5 ratio. This result indicates that [**2**]$(PF_6)_2$ was fully converted into two new species, as the doublets at 9.72 and 9.38 ppm belong to the same species. In addition to these two new species, the signals of free dmbpy (7.86, 7.74, and 7.37 ppm) and free mtpa (singlet at 2.10 ppm) were also found, thus confirming the competing photosubstitution of both dmbpy and mtpa. Although parallel photosubstitution of two distinct ligands has not been described very often, it has been observed recently in our group in a similar complex, [Ru(bpy)(dmbpy)(L-proline)]PF_6 (Chapter 2).[9] These results highlight that methylated ligands are not always the ones that are photosubstituted, and that the selectivity of photosubstitution reactions is the result of a delicate interplay between the energies and shapes of the excited state hypersurfaces that is difficult to predict.

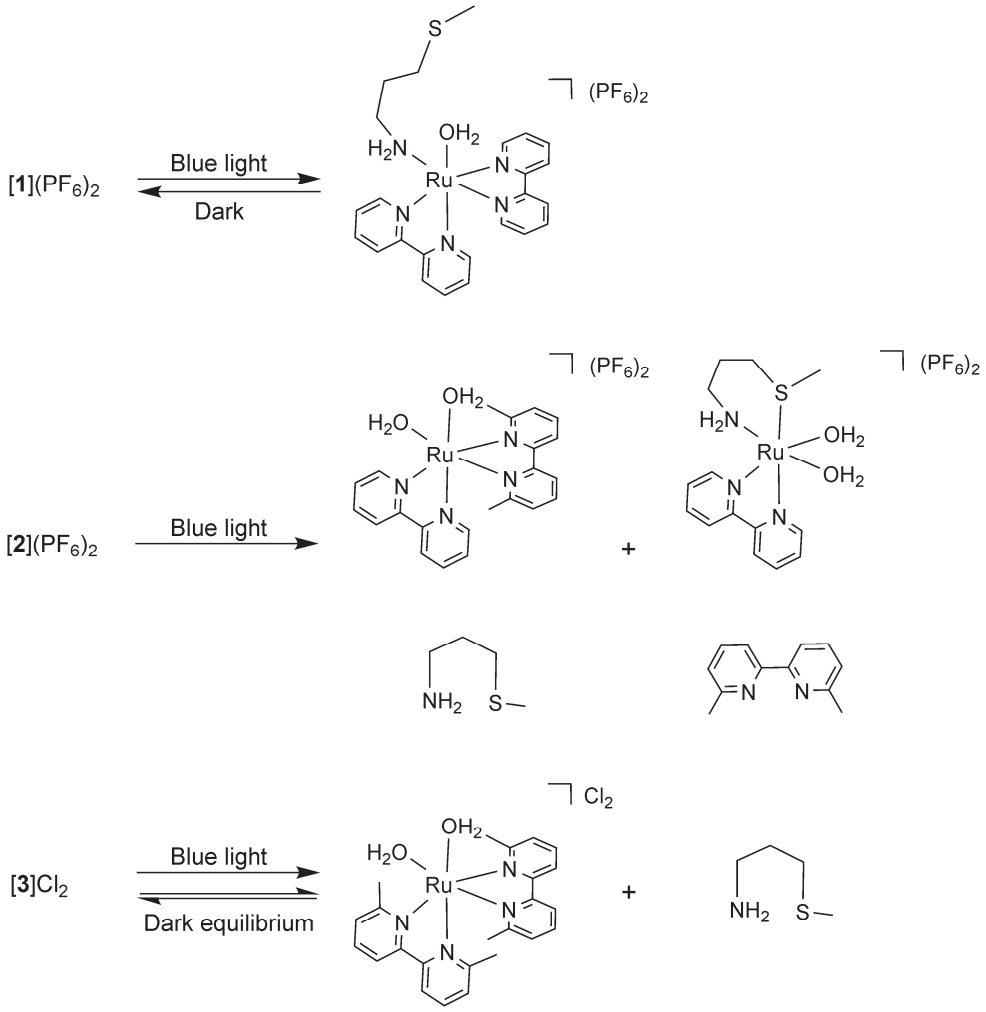

*Scheme 4.2. Photoreaction and thermal equilibria in aqueous solutions of [**1**](PF$_6$)$_2$, [**2**](PF$_6$)$_2$, and [**3**]Cl$_2$.*

4.2.5 Cytotoxicity assays

The cytotoxicity of compounds [**1**](PF$_6$)$_2$, [**2**](PF$_6$)$_2$, [**3**](PF$_6$)$_2$, and of the ligand mtpa was tested against lung cancer cells (A549) following a protocol detailed by Hopkins *et al.*[20] In short, cells were seeded and incubated for 6 h and then treated per triplicate with six different concentrations of the ligand or complexes in two identical plates. After 24 h incubation with the compounds, one of the plates was irradiated with blue light (454 nm), using a light dose of 6.3 J·cm^{-2}, whereas the other plate was kept in the dark. Both plates were further incubated for another 48 h without refreshing the media, and a sulforhodamine assay was performed at t = 96 h. By comparing the cell viability

of treated *vs.* non-treated wells the effective concentrations (EC_{50}), *i.e.* the compound concentration needed to decrease the cell survival to 50% compared to non-treated control, was determined for each compound. Before performing cytotoxicity assays, we first verified that a light dose of 6.3 $J \cdot cm^{-2}$ was *i)* enough to activate all three ruthenium compounds at the highest concentration used in the assays (86 µM solution) and under exactly the same conditions (Figure AV.9), and *ii)* non-toxic to A549 cells.[20] The EC_{50} values in the dark and upon light irradiation are given in Table 4.3.

The free ligand mtpa showed no significant cytotoxicity below 100 µM (Figure AV.10), thus any biological activity of the complexes should be attributed to the metal-containing photoproduct (see Chapter 3). As shown in Figure 4.7a, no significant decrease in the cell population was observed after treatment with complex [**1**]$(PF_6)_2$ both in the dark and after blue light irradiation. On the other hand, complex [**3**]$(PF_6)_2$ showed similar cell viability curves and EC_{50} values in the dark and upon light activation, *i.e.* 51.8 and 43.4 µM, respectively, corresponding to a negligible photo index (PI), *i.e.* the ratio of the EC_{50} value obtained in a dark control and that after light irradiation, of 1.2. Most importantly, use of compound [**2**]$(PF_6)_2$ resulted in a decrease of the EC_{50} value from 110 µM in the dark to 13.8 µM after light activation, corresponding to a PI of 8.

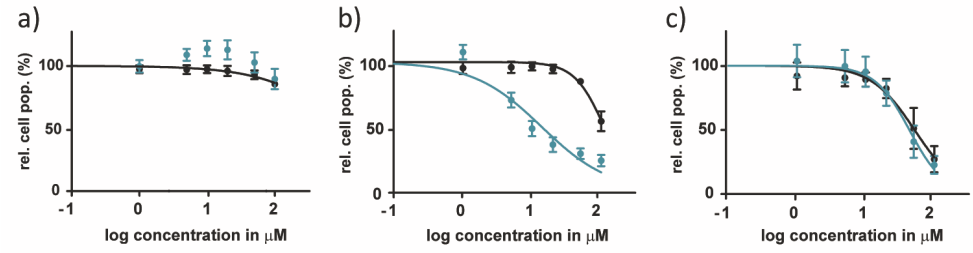

*Figure 4.7. Dose-response curves for A549 cells in presence of a) [**1**](PF$_6$)$_2$, b) [**2**](PF$_6$)$_2$, or c) [**3**](PF$_6$)$_2$ irradiated with blue light (454 nm, 6.35 J·cm^{-2}) 6 h after treatment (blue data points) or left in the dark (black data points). Phototoxicity assay outline: cells seeded at 5·10^3 cells/well at t = 0 h, treated with [**1**](PF$_6$)$_2$, [**2**](PF$_6$)$_2$, or [**3**](PF$_6$)$_2$ at t =24 h, irradiated at t = 30 h, and SRB cell-counting assay performed at t = 96 h. Incubation conditions: 37 °C and 7.0% CO$_2$.*

*Table 4.3. (Photo)cytotoxicity (EC_{50} with confidence interval (CI) (95%) in μM) of [**1**]$(PF_6)_2$, [**2**]$(PF_6)_2$, [**3**]$(PF_6)_2$, and mtpa on A549 cells, and photo indices (PI) defined as EC_{50} dark/EC_{50} light.*

	[1]$(PF_6)_2$	CI (95%)	[2]$(PF_6)_2$	CI (95%)	[3]$(PF_6)_2$	CI (95%)	mtpa	CI (95%)
EC_{50} dark (μM)	>150	-	110	+15	51.8	+12.2	>150	-
		-		−13		−9.9		-
EC_{50} light (μM)	>150	-	13.8	+4.6	43.5	+9.2	>150	-
		-		−3.4		−7.6		-
PI	-		8.0		1.2		-	

4.3 Discussion

While many polypyridyl ruthenium complexes bearing a thioether-based ligand have been reported, to our knowledge only few publications pay attention to the stereoselectivity of the binding of the sulfur atom. For example, Sauvage *et al.* reported on the synthesis of $[Ru(phen)_2(Ph\text{-}S\text{-}(CH_2)_n\text{-}S\text{-}Ph)](PF_6)_2$ (where phen = 1,10-phenanthroline, Ph = phenyl, and n = 2 or 3), for which the single diastereoisomer Λ-*R,R*/Δ-*S,S* is formed and suggested that the reason of this stereoselectivity was the π-π interactions between the phenyl group and the phen ligand, which stabilize the structure.[21] A deeper study from Connick *et al.* suggested that this configuration was also favored by the reduced steric repulsion between the phenyl groups and the H_α atoms of the polypyridyl ligands compared to the other possible configurations.[22] Thus, interligand interactions are crucial in determining the configuration of the sulfur. However, Tresoldi *et al.* consider the isomers of $[Ru(bpy)_2(2\text{-mpps})]^{2+}$ (2-mpps = 2-methylpyridyl pyridyl sulfide) resulting from the inversion of the chiral coordinated sulfur as invertomers.[23] According to this group, fast inversion occurs at room temperature, making the distinction of the invertomers by ^{1}H NMR impossible since only a single set of broad peaks is visible, while in some cases the inversion becomes slower at lower temperatures and the NMR peaks split.[23-24] This second option can be discarded for [**1**]$(PF_6)_2$, as no significant change in the NMR peaks was observed between 193 K and 333 K.

Overall, our data suggest that activation of the mtpa-based complexes via thermal- or light-induced substitution of one of the bidentate ligands by two water molecules is the key factor leading to cytotoxicity. According to spectroscopic studies [**1**]$(PF_6)_2$ is indeed not fully "activated" upon light irradiation, as only the thioether part of the mtpa

ligand is substituted by one water molecule, without formation of the bis-aqua complex. This result, together with the probable low cellular uptake of complexes of that kind,[8] may explain the absence of cytotoxicity after light activation. On the other hand, [**3**]$(PF_6)_2$ shows similar cytotoxicity in the dark and upon light irradiation because formation of the bis-aqua complex by substitution of mtpa occurs already in the dark. In other terms, it is too strained to be thermally stable, which prevents light activation by photosubstitution to be efficient. However, a greater difference in EC_{50} values between dark and irradiated conditions may be expected because the thermal equilibrium between [**3**]$(PF_6)_2$ and the bis-aqua complex is shifted towards the bis-aqua complex by light. Considering the dynamics of speciation in a cell, the different modes by which the drug may be taken up, and the different localization of the prodrug and of the activated drug, it is difficult to claim that equilibrium shifts observed in a simple water solution can replicate in a cell and explain minute cytotoxicity differences between dark and irradiated conditions. However, it is clear that the compound with intermediate steric hindrance and intermediate lipophilicity, *i.e.* [**2**]$(PF_6)_2$, shows at the same time a significant PI, a high thermal stability compared to [**3**]$(PF_6)_2$, and a better photoreactivity compared to [**1**]$(PF_6)_2$. This complex seems thus to be the optimal trade-off between stability and photoreactivity in this family of complexes.

4.4 Conclusions

In this work, we have successfully synthesized a series of complexes bearing the non-toxic thioether mtpa ligand as caging ligand for the bis-aqua species. However, mtpa is a prochiral and dissymmetric ligand, which potentially generates many isomers once coordinated to a ruthenium center. The characterization of the isomer(s) effectively obtained in solution required a combination of crystallography, NOESY spectroscopy, and DFT calculations. In addition, while the non-strained complex $[\mathbf{1}]^{2+}$ is not capable of fully releasing mtpa, the more strained complexes $[\mathbf{2}]^{2+}$ and $[\mathbf{3}]^{2+}$, like dmbpy-based analogues, show efficient mtpa photosubstitution upon blue light irradiation, which in the mildly strained compound [**2**]$(PF_6)_2$ leads to effective light activation in cancer cells. However, when fine-tuning steric hindrance and introducing two different "spectator" bipyridyl ligands, we have lost the selectivity of the photosubstitution reaction in [**2**]$(PF_6)_2$, as both dmbpy and mtpa are substituted by water molecules. Thus, we cannot attribute the enhanced photocytotoxicity of [**2**]$(PF_6)_2$ solely to the photochemically generated *cis*-$[Ru(bpy)(dmbpy)(OH_2)_2]^{2+}$ species, because dmbpy is also toxic (see Chapter 3), and because *cis*-$[Ru(bpy)(mtpa)(OH_2)_2]^{2+}$ is photoreleased as well, the biological properties of which are unknown. Overall, adding methyl groups

in hindering position on the bipyridine ligands does allow for fine-tuning the lipophilicity and photoreactivity of light-activated ruthenium anticancer complexes, but achieving selective substitution of a non-toxic ligand to study the biological properties of a single metal-based photoproduct remains a chemical challenge.

4.5 Experimental

4.5.1 Synthesis

General: The ligands 2,2'-bipyridine (bpy), 6,6'-dimethyl-2,2'-bipyridine (dmbpy), and 3-(methylthio)propylamine (mtpa) were purchased from Sigma-Aldrich, as well as *cis*-bis(2,2′-bipyridine)dichlororuthenium(II) hydrate (*cis*-$[Ru(bpy)_2Cl_2]$). Silver nitrate ($AgNO_3$) and potassium hexafluoridophosphate (KPF_6) were purchased from Alfa-Aesar. Triethylamine (Et_3N) was purchased from Merck. All reactants and solvents were used without further purification. The syntheses of *cis*-$[Ru(dmbpy)_2Cl_2]$, *rac*-$[Ru(bpy)(dmbpy)_2](PF_6)_2$ ([**5**]$(PF_6)_2$), and *rac*-$[Ru(bpy)(dmbpy)(CH_3CN)_2](PF_6)_2$ ([**4**]$(PF_6)_2$) were carried out according to literature procedures.[9, 25] Sephadex LH-20 was used for the Size Exclusion Column (SEC) chromatography. Electrospray mass spectra (ES MS) were recorded by using a Thermoquest Finnagen AQA Spectrometer and a MSQ Plus Spectrometer. All ^1H NMR spectra were recorded on a Bruker DPX-300 or DMX-400 spectrometers. Chemical shifts are indicated in ppm relative to the residual solvent peak.

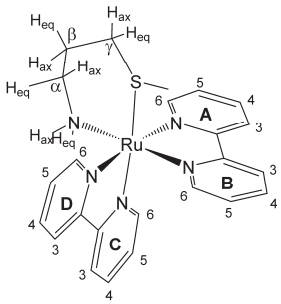

$[Ru(bpy)_2(mtpa)](PF_6)_2$ ([**1**]$(PF_6)_2$). *cis*-$[Ru(bpy)_2Cl_2]$ (49 mg, 0.10 mmol) and $AgNO_3$ (37 mg, 0.21 mmol) were added to deaereted water (10 mL) and stirred at 90 ºC for 30 min. After the solution was filtered to remove the grey solid formed (AgCl), Et_3N (17 µL, 0.12 mmol) and mtpa (14 µL, 0.12 mmol) were added to the filtrate, which was stirred at 90 ºC for 1 h under Ar. Then, after addition of saturated KPF_6 aqueous solution an orange precipitate was obtained. After filtration, the product was purified by SEC chromatography using CH_3OH as eluent. The main orange fraction

was collected and, after solvent evaporation, an orange solid was obtained. Yield: 40 mg (50%). Two isomers in a ratio 1:0.05. ^{1}H NMR of the major isomer (Λ-(*S*), Δ-(*R*))-[**1**](PF$_6$)$_2$ (400 MHz, D$_2$O) δ 9.79 (d, J = 5.7 Hz, 1H, D6), 9.23 (d, J = 5.3 Hz, 1H, A6), 8.54 (m, 2H, A3 + D3), 8.41 (d, J = 8.2 Hz, 1H, C3), 8.35 (d, J = 8.2 Hz, 1H, B3), 8.25 (t, J = 8.0 Hz, 1H, A4), 8.20 (td, J = 7.9, 1.5 Hz, 1H, D4), 7.93 (td, J = 7.9, 1.6 Hz, 1H, C4), 7.89 – 7.80 (m, 3H, A5 + B4 + D5), 7.65 (d, J = 5.5 Hz, 1H, B6), 7.56 (d, J = 5.6 Hz, 1H, C6), 7.25 (ddd, J = 7.2, 5.6, 1.4 Hz, 1H, C5), 7.14 (ddd, J = 7.2, 5.6, 1.4 Hz, 1H, B5), 3.92 (d, J = 12.1 Hz, 1H, N_{eq}), 3.17 – 2.92 (m, 3H, γ_{eq} + N_{ax} + α_{ax}), 2.86 – 2.76 (m, 1H, α_{eq}), 2.53 (t, J = 11.7 Hz, 1H, γ_{ax}), 2.28 – 2.15 (m, 1H, β_{eq}), 1.79 – 1.66 (m, 1H, β_{ax}), 1.19 (s, 3H, MeS-). High Resolution ES MS m/z (calcd): 259.55127 (259.55098, [**1**]$^{2+}$), 664.06787 (664.0667, [**1** + PF$_6$]$^+$). Anal. Calcd for $C_{29}H_{32}F_6N_5O_2PRu$: C, 35.65; H, 3.37; N, 8.66 Found: C, 35.67; H, 3.34; N, 8.64

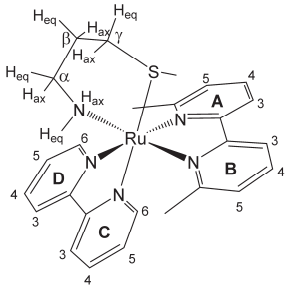

[Ru(bpy)(dmbpy)(mtpa)](PF$_6$)$_2$ ([**2**](PF$_6$)$_2$). [**4**](PF$_6$)$_2$ (50 mg, 0.061 mmol), mtpa (13 μL, 0.12 mmol), and Et$_3$N (45 μL, 0.32 mmol) were dissolved in deaereted water (5 mL) and refluxed under Ar for 2 h, after which the solvent was removed under reduced pressure by rotary evaporation at 40 °C. The crude reaction mixture was purified by an alumina chromatography column using a CH_2Cl_2/CH_3OH mixture in a gradient 0 − 1% of CH_3OH as eluent. The yellow (R_f = 0.65) and orange (R_f = 0.6) fractions were collected and the solvent was removed under reduced pressure by rotary evaporation at 40 °C. Yield: 32 mg (62%). Two isomers in a ratio 1:0.09. ^{1}H NMR of the the major isomer (Λ-(*R*), Δ-(S))-[**2a**](PF$_6$)$_2$ ^{1}H NMR (400 MHz, CD_3OD) δ 9.55 (d, J = 5.4 Hz, 1H, D6), 8.71 (d, J = 7.8 Hz, 1H, D3), 8.65 (d, J = 8.1 Hz, 1H, C3), 8.45 (d, J = 7.8 Hz, 1H, A3), 8.29 (d, J = 7.9 Hz, 1H, B3), 8.25 (td, J = 7.9, 1.4 Hz, 1H, D4), 8.21 (d, J = 5.2 Hz, 1H, C6), 8.17 – 8.10 (m, 2H, A4 + C4), 7.86 – 7.80 (m, 2H, D5 + B4), 7.76 (dd, J = 7.8, 1.3 Hz, 1H, A5), 7.50 (ddd, J = 7.3, 5.7, 1.3 Hz, 1H, C5), 7.21 (dd, J = 7.8, 1.2 Hz, 1H, B5), 3.87 – 3.76 (m, 1H, N_{ax}), 3.14 – 3.01 (m, 2H, N_{eq} + γ_{ax}), 2.92 (s, 3H, AMe), 2.67 – 2.57 (m, 1H, α), 2.53 – 2.43 (m, 1H, γ_{eq}), 2.17 – 2.07 (m, 1H, α), 2.06 – 1.97 (m, 1H, β), 1.96 – 1.87 (m, 1H, β), 1.62 (s, 3H, BMe), 1.58 (s, 3H, MeS-). ^{13}C

NMR (101 MHz, CD_3OD) δ 167.54, 167.01, 161.41, 161.35, 160.57, 159.71, 156.75, 155.03, 139.57, 139.28, 139.17, 138.75, 128.90, 128.39, 128.25, 127.87, 126.08, 125.46, 122.68, 122.46, 42.32, 35.25, 27.17, 26.48, 24.69, 17.74. High Resolution ES MS m/z (calcd): 273.56708 (273.56663, $[\mathbf{2}]^{2+}$), 692.09851 (692.09800, $[\mathbf{2} + PF_6]^+$). Anal. Calcd for $C_{29}H_{32}F_6N_5O_2PRu$: C, 37.33; H, 3.73; N, 8.37 Found: C, 37.41; H, 3.87; N, 8.31

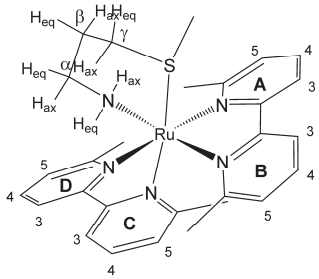

[Ru(dmbpy)$_2$(mtpa)](PF$_6$)$_2$ ([**3**](PF$_6$)$_2$). *cis*-[Ru(dmbpy)$_2$Cl$_2$] (50 mg, 0.093 mmol) was dissolved in deaereted water (3 mL) and heated under Ar at 60 °C for 5 min, after which mtpa (17 μL, 0.16 mmol) and Et_3N (20 μL, 0.14 mmol) were added to the reaction mixture and stirred at 60 °C for 45 min. Then, after addition of saturated KPF_6 aqueous solution (1 mL), a reddish precipitate was obtained. The suspension was filtered and washed with cold water (5 mL) and diethyl ether. Yield: 40 mg (50%). Two isomers in a ratio 1:0.12. ^{1}H NMR of the major isomer (Λ-(*S*), Δ-(*R*))-ax-[**3**](PF$_6$)$_2$ (400 MHz, CD_3OD) δ 8.53 (d, *J* = 7.9 Hz, 1H, D3), 8.50 (d, *J* = 8.2 Hz, 1H, C3), 8.44 (m, 2H, A3 + B3), 8.12 (td, *J* = 7.9, 3.4 Hz, 1H, D4 + A4), 8.06 (t, *J* = 7.9 Hz, 1H, C4), 7.97 (t, *J* = 7.9 Hz, 1H, B4), 7.68 (td, *J* = 7.5, 1.3 Hz, 2H, A5 + D5), 7.45 (d, *J* = 7.8 Hz, 1H, C5), 7.41 (d, *J* = 7.8 Hz, 1H, B5), 3.26 – 3.18 (m, 1H), 2.83 (s, 3H, DMe), 2.75 – 2.68 (m, 1H, γ_{eq}), 2.67 (s, 3H, AMe), 2.50 (d, *J* = 12.6 Hz, 1H), 2.44 – 2.33 (m, 1H, γ_{ax}), 1.94 (s, 3H, BMe), 1.86 (s, 3H, CMe), 1.79 – 1.68 (m, 1H), 1.20 (s, 3H, MeS-), 0.33 (d, *J* = 12.0 Hz, 1H). ^{13}C NMR (101 MHz, acetone-d6) δ 168.21, 167.82, 167.35, 167.27, 161.13, 160.95, 160.34, 160.14, 139.16, 139.03, 138.91, 138.28, 128.15, 127.45, 127.32, 126.93, 124.33, 123.34, 123.04, 122.43, 41.93, 34.74, 26.39, 25.35, 24.60, 24.39, 23.38, 15.62. High Resolution ES MS m/z (calcd): 287.58243 (287.58228, $[\mathbf{3}]^{2+}$), 720.12781 (720.12930, $[\mathbf{3} + PF_6]^+$). Anal. Calcd for $C_{29}H_{32}F_6N_5O_2PRu$: C, 38.89; H, 4.08; N, 8.10 Found: C, 38.02; H, 4.18; N, 7.64

4.5.2 Photochemistry

General: For the irradiation experiments of NMR tubes, the light of a LOT 1000 W Xenon Arc lamp mounted with infrared and 400 nm long pass filters was used. When specified, a 450 nm 450FS10-50 from Andover Corporation filter was used. For NMR experiments under N_2, NMR tubes with PTFE stopper were used. UV-vis experiments were performed on a Cary 50 Varian spectrometer. When monitoring photoreactions by UV-vis and mass spectrometry, a LED light source (λ_{ex} = 445 nm, with a Full Width at Half Maximum of 14 nm, Part. No H2A1-H450, Roithner LaserTechnik, Vienna, Austria) with a light intensity between $2.79 \cdot 10^{-8}$ and $2.98 \cdot 10^{-8}$ mol·s^{-1} was used.

Experiments monitored with ^{1}H NMR: A stock solution in deuterated water of either [**1**]$(PF_6)_2$, [**2**]$(PF_6)_2$, or [**3**]Cl_2 was prepared and deaereted under N_2 (see Table 4.4 for the details). Then, 600 µL of the stock solution were transferred, under N_2, into a NMR tube. The tube was irradiated at room temperature with a LOT Xenon 1000 W lamp equipped with IR short pass and >400 nm long pass filters. In addition, a control experiment without white light irradiation was performed. The reactions were monitored with ^{1}H NMR at various time intervals.

*Table 4.4. Conditions of the photoreactions of [**1**]$(PF_6)_2$, [**2**]$(PF_6)_2$, and [**3**]Cl_2 in D_2O monitored with ^{1}H NMR.*

Complex	w (mg)	V (µL)	Mw (g/mol)	Concentration (mM)
[**1**]$(PF_6)_2$	1.6	660	808.57	3.0
[**2**]$(PF_6)_2$	1.0	600	836.63	2.0
[**3**]Cl_2[a]	1.0	600	645.65	2.6

[a] *Complex [**3**]$(PF_6)_2$ was converted to [**3**]Cl_2 for solubility reasons by addition of Bu_4NCl in acetone, followed by filtration and washing with cold acetone and diethyl ether.*

Irradiation experiments monitored with UV-vis and MS: UV-vis spectroscopy was performed using a UV-vis spectrometer equipped with temperature control set to 25 or 37 ºC and a magnetic stirrer. The irradiation experiments were performed in a quartz cuvette containing 3 mL of solution. A stock solution of the desired complex was prepared using demineralized water, which was then diluted in the cuvette to a working solution concentration. When the experiment was carried out under N_2 the sample was deaereted 15 min by gentle bubbling of N_2 and the atmosphere was kept inert during the experiment by a gentle flow of N_2 on top of the cuvette. A UV-vis spectrum was measured every 30 s for the first 10 min, every 1 min for the next 10 min, and eventually every 10 min until the end of the experiment. Data was analysed with Microsoft Excel. Experimental conditions are detailed in Table 4.5.

*Table 4.5. Conditions of the photoreactions of **[1]**$(PF_6)_2$, **[2]**$(PF_6)_2$, and **[3]**Cl_2 in demineralized water monitored with MS and UV-vis.*

Complex	Stock solution				Working solution (mM)	Photon flux 445 nm LED ($mol \cdot s^{-1}$)	Temperature (°C)
	w (mg)	V (mL)	M_w (g/mol)	M (mM)			
[1]$(PF_6)_2$	2.4	10	808.57	0.297	0.145	$2.95 \cdot 10^{-8}$	25
					0.099	$2.91 \cdot 10^{-8}$	37
[2]$(PF_6)_2$	0.6	5	836.63	0.151	0.101	$2.92 \cdot 10^{-8}$	25
[3]Cl_2[a]	1.6	10	645.65	0.245	0.123	$2.79 \cdot 10^{-8}$	25

[a] *Complex **[3]**$(PF_6)_2$ was converted to **[3]**Cl_2 for solubility reasons by addition of Bu_4NCl in acetone, followed by filtration and washing with cold acetone and diethyl ether.*

Blue light irradiation in the cell irradiation setup: The photochemical reactivity of [**1**]$(PF_6)_2$, [**2**]$(PF_6)_2$, and [**3**]$(PF_6)_2$ in 96-well plates was measured using UV-vis spectroscopy. Solutions of each compound were prepared in OptiMEM complete (86 μM), transferred into a 96-well plate, and irradiated with blue light (454 nm) at different irradiation times using the blue LED source described in details in Hopkins *et al*. to mimic the conditions used in the photocytotoxicity assay.[20] Figure AV.9 shows that the three complexes are fully activated at 86 μM after 10 min irradiation. Thus, 10 min was chosen as the blue light irradiation time in the photocytotoxity assay, which corresponded to a light dose of 6.3 $J.cm^{-2}$.

4.5.3 Single Crystal X-Ray crystallography

General: All reflection intensities were measured at 110(2) K using a SuperNova diffractometer (equipped with Atlas detector) with Cu *K*α radiation (λ = 1.54178 Å) or Mo *K*α radiation (λ = 0.71073 Å) under the program CrysAlisPro (Version 1.171.36.32 Agilent Technologies, 2013). The same program was used to refine the cell dimensions and for data reduction. The structure was solved with the program SHELXS-2013 and was refined on F^2 with SHELXL-2013.[26] Analytical numeric absorption correction based on a multifaceted crystal model was applied using CrysAlisPro. The temperature of the data collection was controlled using the system Cryojet (manufactured by Oxford Instruments). The H atoms were placed at calculated positions (unless otherwise specified) using the instructions AFIX 23, AFIX 43, AFIX 137 or AFIX 147 with isotropic displacement parameters having values 1.2 *U*eq of the attached C or O atoms.

Complex [1]$(PF_6)_2 \cdot CH_3OH$

Crystal growing: [**1**]$(PF_6)_2$ (1.0 mg) was dissolved in CH_3OH (1 mL, 1.2 mM) in a GC vial, which was placed in a larger vial that contained toluene (3 mL) as a counter

solvent. The large vial was stoppered. After a few days, quality crystals suitable for X-ray structure determination were obtained by vapour diffusion.

Crystal structure determination: The H atoms attached to N5 were found from difference Fourier maps, and their coordinates and isotropic temperature factors were refined freely.

Details of the crystal structure: The structure is mostly ordered. The lattice CH_3OH solvent molecule is disordered over two orientations and the occupancy factor of the major component of the disorder refines to 0.70(2). Fw = 840.62, red block, 0.38 × 0.28 × 0.25 mm^3, monoclinic, *C*2/*c* (no. 15), a = 12.5589(2), b = 14.0651(2), c = 36.3739(7), β = 98.5152(18)°, V = 6354.34(19) $Å^3$, Z = 8, D_x = 1.757 g cm^{-3}, μ = 6.502 mm^{-1}, T_{min}–T_{max}: 0.224–0.383. 20578 Reflections were measured up to a resolution of $(\sin \theta/\lambda)_{max}$ = 0.62 $Å^{-1}$. 6232 Reflections were unique (R_{int} = 0.0175), of which 6168 were observed [$I > 2\sigma(I)$]. 449 Parameters were refined using 37 restraints. *R*1/*wR*2 [$I > 2\sigma(I)$]: 0.0335/0.0811. *R*1/*wR*2 [all refl.]: 0.0339/0.0814. S = 1.147. Residual electron density found between −0.68 and 0.84 e $Å^{-3}$.

Complex [2a](PF$_6$)$_2$

Crystal growing: [**2**](PF$_6$)$_2$ (1.0 mg) was dissolved in CH_3OH (1 mL. 1.2 mM) in a GC vial, which was placed in a larger vial that contained ethyl acetate (3 mL) as a counter solvent. The large vial was stoppered. After few days, quality crystals suitable for X-ray structure determination were obtained by vapour diffusion.

Crystal structure determination: The H atoms attached to N5 were found from difference Fourier map, and their coordinates and isotropic temperature factors were refined freely. The structure is partly disordered.

Details of the crystal structure: One of the two PF_6^- counter ions is disordered over 3 orientations. The occupancy factors of the three different orientation can be retrieved in the .cif file. Fw = 836.63, 0.24 × 0.21 × 0.07 mm^3, orthorhombic, Pbca, a = 9.17330(14), b = 18.2183(3), c = 36.9112(5), V = 6168.67(16) $Å^3$, Z = 8, μ = 6.67 mm^{-1}, T_{min}–T_{max}: 0.331–0.673. 36039 Reflections were measured up to a resolution of $(\sin \theta/\lambda)_{max}$ = 0.616 $Å^{-1}$. 6052 Reflections were unique (R_{int} = 0.039), of which 5360 were observed [$I > 2\sigma(I)$]. 552 Parameters were refined using 619 restraints. $R[F^2 > 2\sigma(F^2)]$: 0.028. $wR(F^2)$: 0.067. S = 1.04. Residual electron density found between −0.58 and 0.56 e $Å^{-3}$.

Complex [3](PF$_6$)$_2$

Crystal growing: [**3**](PF$_6$)$_2$ (1.0 mg) was dissolved in CH$_3$OH (1 mL, 1.2 mM) in a GC vial, which was placed in a larger vial that contained di-*tert*-butyl ether (3 mL) as a counter solvent. The large vial was stoppered. After few days, quality crystals suitable for X-ray structure determination were obtained by vapour diffusion.

Crystal structure determination: The structure is partly disordered.

Details of the crystal structure: One of the two PF_6^- counterions is found to be disordered over three orientations, and the occupancy factors of the three components refine to 0.732(3), 0.180(3) and 0.088(3). Fw = 864.68, 0.21 × 0.16 × 0.05 mm^3, triclinic, P-1, a = 10.6739(3), b = 11.7852(3), c = 14.2773(4), V = 1662.91(8) Å^3, Z = 2, μ = 0.73 mm^{-1}, T_{min}–T_{max}: 0.661–1.000. 25022 Reflections were measured up to a resolution of (sin $\theta/\lambda)_{max}$ = 0.650 Å^{-1}. 7639 Reflections were unique (R_{int} = 0.038), of which 6580 were observed [$I > 2\sigma(I)$]. 564 Parameters were refined using 253 restraints. $R[F^2 > 2\sigma(F^2)]$: 0.035. $wR(F^2)$: 0.078. S = 1.03. Residual electron density found between −0.52 and 1.14 e Å^{-3}.

4.5.4 DFT calculations

Electronic structure calculations were performed using DFT as implemented in the ADF program (SCM). The structures of all possible isomers of [**1**]$^{2+}$, [**2a**]$^{2+}$, [**2b**]$^{2+}$, and [**3**]$^{2+}$ were optimized in water using the conductor-like screening model (COSMO) to simulate the effect of solvent. The PBE0 [31] functional and a triple zeta potential basis set (TZP) were used for all calculations.

4.5.5 Cell culture and EC50 (photo)cytotoxicity assay

Following the protocol described in Appendix II, A549 cells were seeded at t = 0 h, and 24 h after aliquots (100 µL) of six different concentrations (1 – 100 µM for all the compounds) of freshly prepared stock solutions of [**1**](PF$_6$)$_2$, [**2**](PF$_6$)$_2$, [**3**](PF$_6$)$_2$, or mtpa in OptiMEM were added. Plates were incubated in the dark for an additional 6 h. After this period, half of the plates were irradiated for 10 min with blue light (λ = 454 ± 11 nm, power density = 10.5 ± 0.7 mW cm^{-2}, irradiation time = 10 min, light dose = 6.5 J·cm^{-2}) and the other half were kept in the dark. After irradiation, all the plates were incubated for an additional 66 h (making a total assay of 96 h).

4.6 References

1. G. Shi, S. Monro, R. Hennigar, J. Colpitts, J. Fong, K. Kasimova, H. Yin, R. DeCoste, C. Spencer, L. Chamberlain, A. Mandel, L. Lilge and S. A. McFarland, *Coord. Chem. Rev.*, **2015**, 282–283, 127-138.
2. H. Huang, B. Yu, P. Zhang, J. Huang, Y. Chen, G. Gasser, L. Ji and H. Chao, *Angew. Chem., Int. Ed.*, **2015**, 54, 14049-14052.
3. V. Pierroz, R. Rubbiani, C. Gentili, M. Patra, C. Mari, G. Gasser and S. Ferrari, *Chem. Sci.*, **2016**, 7, 6115-6124.
4. E. Wachter, D. K. Heidary, B. S. Howerton, S. Parkin and E. C. Glazer, *Chem. Commun.*, **2012**, 48, 9649-9651.
5. R. N. Garner, J. C. Gallucci, K. R. Dunbar and C. Turro, *Inorg. Chem.*, **2011**, 50, 9213-9215.
6. B. S. Howerton, D. K. Heidary and E. C. Glazer, *J. Am. Chem. Soc.*, **2012**, 134, 8324-8327.
7. T. Sainuddin, M. Pinto, H. Yin, M. Hetu, J. Colpitts and S. A. McFarland, *J. Inorg. Biochem.*, **2016**, 158, 45-54.
8. J. A. Cuello-Garibo, M. S. Meijer and S. Bonnet, *Chem. Commun.*, **2017**, 53, 6768-6771.
9. J.-A. Cuello-Garibo, E. Pérez-Gallent, L. van der Boon, M. A. Siegler and S. Bonnet, *Inorg. Chem.*, **2017**, 56, 4818-4828.
10. R. E. Goldbach, I. Rodriguez-Garcia, J. H. van Lenthe, M. A. Siegler and S. Bonnet, *Chem. - Eur. J.*, **2011**, 17, 9924-9929.
11. A. Bahreman, B. Limburg, M. A. Siegler, E. Bouwman and S. Bonnet, *Inorg. Chem.*, **2013**, 52, 9456-9469.
12. R. N. Garner, L. E. Joyce and C. Turro, *Inorg. Chem.*, **2011**, 50, 4384-4391.
13. M. E. Fleet, *Mineral. Mag.*, **1976**, 40, 531-533.
14. V. H. S. van Rixel, B. Siewert, S. L. Hopkins, S. H. C. Askes, A. Busemann, M. A. Siegler and S. Bonnet, *Chem. Sci.*, **2016**.
15. O. Filevich, M. Salierno and R. Etchenique, *J. Inorg. Biochem.*, **2010**, 104, 1248-1251.
16. R. Arakawa, S. Tachiyashiki and T. Matsuo, *Anal. Chem.*, **1995**, 67, 4133-4138.
17. L. Zayat, O. Filevich, L. M. Baraldo and R. Etchenique, *Philos. Trans. R. Soc., A*, **2013**, 371.
18. S. Tachiyashiki and K. Mizumachi, *Coord. Chem. Rev.*, **1994**, 132, 113-120.
19. A. Bahreman, B. Limburg, M. A. Siegler, R. Koning, A. J. Koster and S. Bonnet, *Chem. - Eur. J.*, **2012**, 18, 10271-10280.
20. S. L. Hopkins, B. Siewert, S. H. C. Askes, P. Veldhuizen, R. Zwier, M. Heger and S. Bonnet, *Photochem. Photobiol. Sci.*, **2016**, 15, 644-653.
21. J. P. Collin, D. Jouvenot, M. Koizumi and J. P. Sauvage, *Inorg. Chim. Acta*, **2007**, 360, 923-930.
22. N. A. F. Al-Rawashdeh, S. Chatterjee, J. A. Krause and W. B. Connick, *Inorg. Chem.*, **2014**, 53, 294-307.
23. G. Tresoldi, L. Baradello, S. Lanza and P. Cardiano, *Eur. J. Inorg. Chem.*, **2005**, 2005, 2423-2435.
24. G. Tresoldi, S. Lo Schiavo, S. Lanza and P. Cardiano, *Eur. J. Inorg. Chem.*, **2002**, 2002, 181-191.
25. J. P. Collin and J. P. Sauvage, *Inorg. Chem.*, **1986**, 25, 135-141.
26. G. M. Sheldrick, *Acta Crystallogr., Sect. A: Found. Adv.*, **2008**, 64, 112-122.